 DOI: 10.1002/eji.201646291 Eur. J. Immunol. 2016. 46: 2376–2387

Basic

European Journal of Immunology

Molecular immunology and signaling

Research Article

Clathrin regulates lymphocyte migration by driving actin accumulation at the cellular leading edge

Guillermo Ramírez-Santiago[1,2], Javier Robles-Valero[3], Giulia Morlino[3], Aranzazu Cruz-Adalia[1,2], Manuel Pérez-Martínez[4], Airen Zaldivar[5], Mónica Torres-Torresano[1,2], Francisco Javier Chichón[5], Andrea Sorrentino[6], Eva Pereiro[6], José L. Carrascosa[5,7], Diego Megías[4], Carlos Oscar S. Sorzano[5], Francisco Sánchez-Madrid[3] and Esteban Veiga[1,2]

[1] Centro Nacional de Biotecnología, Consejo Superior de Investigaciones Científicas (CNB-CSIC), Department of Molecular & Cellular Biology, Madrid, Spain
[2] Instituto de Investigación Sanitaria Princesa, Hospital de Santa Cristina, Madrid, Spain
[3] Instituto de Investigación Sanitaria Princesa, Hospital de la Princesa, Madrid, Spain
[4] Centro Nacional de Investigaciones Oncológicas (CNIO), Madrid, Spain
[5] Centro Nacional de Biotecnología (CNB-CSIC), Department of Macromolecular Structures, Madrid, Spain
[6] ALBA Synchrotron Light Source, MISTRAL Beamline—Experiments Division, Cerdanyola del Vallès, Barcelona, Spain
[7] Unidad Asociada CNB (CSIC)-Instituto Madrileño de Estudios Avanzados en Nanociencia (IMDEA Nanociencia), Cantoblanco, Madrid, Spain

Lymphocyte migration, which is essential for effective immune responses, belongs to the so-called amoeboid migration. The lymphocyte migration is up to 100 times faster than between mesenchymal and epithelial cell types. Migrating lymphocytes are highly polarized in three well-defined structural and functional zones: uropod, medial zone, and leading edge (LE). The actiomyosin-dependent driving force moves forward the uropod, whereas massive actin rearrangements protruding the cell membrane are observed at the LE. These actin rearrangements resemble those observed at the immunological synapse driven by clathrin, a protein normally involved in endocytic processes. Here, we used cell lines as well as primary lymphocytes to demonstrate that clathrin and clathrin adaptors colocalize with actin at the LE of migrating lymphocytes, but not in other cellular zones that accumulate both clathrin and actin. Moreover, clathrin and clathrin adaptors, including Hrs, the clathrin adaptor for multivesicular bodies, drive local actin accumulation at the LE. Clathrin recruitment at the LE resulted necessary for a complete cell polarization and further lymphocyte migration in both 2D and 3D migration models. Therefore, clathrin, including the clathrin population associated to internal vesicles, controls lymphocyte migration by regulating actin rearrangements occurring at the LE.

Keywords: Cellular immunology · Cytoskeleton · Lymphocyte migration

Additional supporting information may be found in the online version of this article at the publisher's web-site

Correspondence: Dr. Esteban Veiga
e-mail: eveiga@cnb.csic.es

Introduction

Lymphocyte migration to sites of infection or injury is essential for an effective immune response [1]. Contrary to the slow mesenchymal mode of migration defining by strong anchoring to the substrate, leukocytes (amoeboid) migration resembles that of the amoeba *Dictyostelium discoideum* [2], reaching speeds up to 100 times faster than mesenchymal and epithelial cell types [3]. Lymphocyte migration is driven by protrusion and contraction, and is defined by constant shape changes and cellular polarization in three well-defined zones; a very dynamic actin-rich leading edge (LE), a central cell body, and the uropod, which is the posterior tail [4]. The uropod, where there are located the mitochondria, provides the actin/myosin-dependent pushing force, whereas the branched actin networks formed at the LE push the plasma membrane protruding it outward. Interestingly, there exist increasing pieces of evidence showing that clathrin, extensively studied by its central role in endocytosis [5], has been associated during different biological processes involving local actin remodeling such as pathogen infections [6, 7], membrane invaginations [8], and lamellipodium formation [9] among others. Moreover, it has been shown that during antigen presentation, clathrin not only participates in the same events that requires actin remodeling, but drives itself local and massive actin accumulation observed in T cells contacting antigen-loaded antigen presenting cells [10].

Here, using up to date imaging technologies, and developing ad hoc image analysis software, we show that clathrin plays a pivotal role in actin remodeling observed at the LE of migrating cells during amoeboid migration. Clathrin recruitment to the cellular front resulted essential for a proper lymphocyte polarization and further migration. We also show that clathrin population involved in T-cell migration are linked to plasma membrane as well as to internal vesicles and we show these data using lymphoid cells lines as well as human primary T cells.

Results

To test the localization of clathrin, clathrin adaptors (clathrin bind to different cell membranes through interaction with proteins called clathrin adaptors [11, 12]), and actin in migrating lymphocytes, we used a model of 2D migration based in the human T-cell line CEM (C.E.M. are the initials of the child with acute lymphoblastic leukemia from whom the lymphocytes were isolated from periferal blood and cultured) plated on glass cover slides in the presence of stromal cell derived factor 1α (SDF-1α). This model of chemokine-dependent migration has been previously used to study cellular migration [13, 14]. Cells were transfected with td-Tomato-LCa (clathrin light chain fused to td-Tomato) and GFP–actin and monitored by confocal microscope. Upon SDF-1α addition, cells polarized, start migrating, and a clear accumulation of clathrin is observed not only at the uropod, where it was described to be [15], but also at the LE, mirroring actin (Supporting Information Movies 1 and 2). The presence of endogenous clathrin at the LE of migrating lymphocyte, together with actin (detected using fluorescent Phalloidin), was confirmed by immunofluorescence using antibodies against clathrin heavy chain (Fig. 1A). We also analyzed the subcellular location of Hrs, the clathrin adaptor that connects clathrin with multivesicular bodies (MVBs), which has been shown to play a major role in actin accumulation at the immunological synapse (IS) [10] (Fig. 1B). Hrs accumulation paralleled that of clathrin, and can be detected together with actin in both the uropod and the LE of migrating T cells. Dynamin 2, a large GTPase that links clathrin and actin [16] and promotes actin polymerization at the IS [17], was also localized at the LE of migrating lymphocytes (Fig. 1C). To quantify the localization of these proteins, we performed colocalization analysis that showed that clathrin (Fig. 1D) and Hrs (Fig. 1E) colocalized with actin at the LE but not in the uropod, indicating that clathrin (and clathrin associated to internal vesicles) in the LE is linked to actin polymerization. A scheme indicating the different zones in which a migrating lymphocyte is divided, that is, LE, middle part of the cell, and uropod, is shown Figure 1F.

In order to follow the recruitment dynamics of clathrin-coated vesicles toward the LE, we performed live cell imaging of migrating lymphocytes. Lymphocytes were transfected with td-Tomato-LCa and monitored by epifluorescence microscope (Supporting Information Movie 3). Vesicle-tracking analysis shows that vesicles in the LE behave differently than those found in the uropod or in static cells (Fig. 2A–D), vesicle displacement length and directionality in the LE are compatible with actin-driven vesicle movement [18].

The ultrastructure of the LE of migrating lymphocytes was further assessed by cryo-soft-X-ray tomography, a novel technology that allows to visualize cellular organization at high resolution in a hydrated state the whole cells, avoiding embedding, dehydration, and sectioning artifacts [19]. A tomogram reconstruction of migrating lymphocyte can be observed in Figure 2E–G. Mitochondria, the microtubule-organizing center, and other organelles can be observed in the uropod, behind the nucleus. In the LE, vesicles appeared associated with filaments, which are compatible, by size, with actin filaments, in agreement with what is shown in Figure 1.

Clathrin drives actin accumulation at the LE of migrating lymphocytes

In order to test whether clathrin recruitment is necessary for further actin accumulation at the LE of migrating T cells, we knocked down clathrin and clathrin adaptors by siRNA (Fig. 3A). Clathrin or Hrs silencing did not affect the surface expression of CXCR4 (Fig. 3B), the receptor of SDF-1α that would promote cell polarization and migration [20]. Clathrin silencing, however, resulted in a decrease of total actin polymerization in migrating cells measured by flow cytometry (Fig. 3C). Further quantification of actin accumulation at the LE was performed by image analysis of fluorescent confocal images using "FluorescenceRatio," ad hoc homemade software, further described in Methods section, developed as a plug-in for ImageJ (NIH; Bethesda, MD); briefly, the fluorescence of F-actin at the LE was compared with the fluorescence

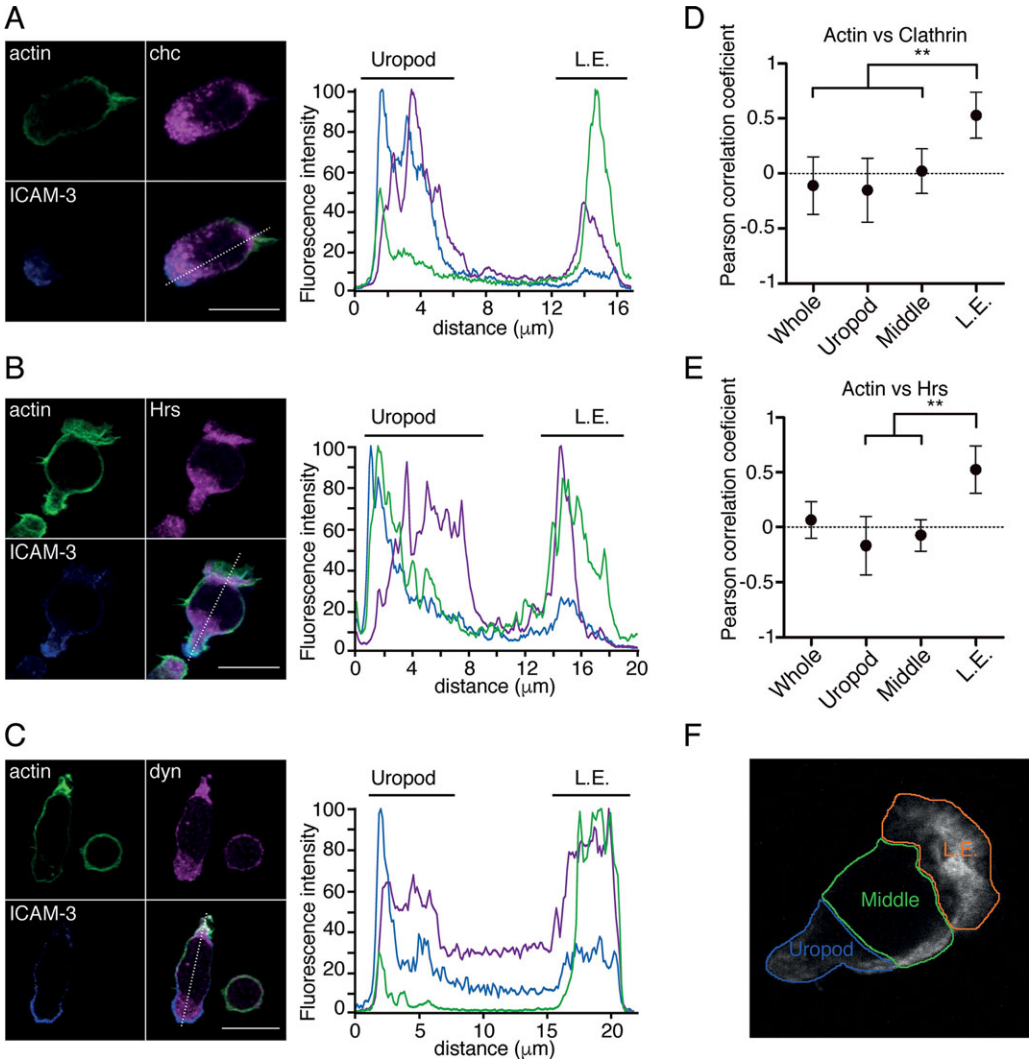

Figure 1. Clathrin and actin colocalize at the LE of migrating human cell line CEM. (A–C) Migrating CEM cells were stained for the indicated proteins (CHC; actin [detected using fluorescent phalloidin]; Hrs; and dynamin 2, dyn) and (left) imaged by confocal microscopy; uropod is marked with ICAM-3. (Right) Fluorescence intensity analysis was performed from the uropod to the LE over the line represented at the merge image. Images and graphs are representative of five independent experiments, with $n = 50$ samples each. (D and E) Colocalization analysis for actin and clathrin (D) or actin and clathrin adaptor protein Hrs (E) represented as Pearson correlation coefficient. (D and E) Data shown are pooled from four different experiments each one measuring at least 10 cells. (F). Scheme showing the different cell areas considered in the colocalization analysis.

detected in the uropod (Fig. 3D). Actin accumulation at the LE in migrating control cells was detected to be three times larger than actin accumulation in the uropod; however, clathrin-silenced cells totally lost actin accumulation at the LE (Fig. 3E). Silencing Hrs and the clathrin adaptor for the plasma membrane, AP-2, also reduced actin accumulation at the LE of migrating T cells. On the contrary, silencing AP-1, clathrin adaptor for the Golgi apparatus, had no effect in actin polymerization (Fig. 3E). These data confirm that plasma membrane clathrin and the clathrin population associated with internal vesicles are necessary not only for providing membranes at the LE [15], but also for further actin accumulation at the front of migrating lymphocytes. Accumulation of arp2 (the arp2/3 complex is the major actin-polymerizing actor, promoting actin polymerization in branched ends [21, 22]; Fig. 3F) and dynamin 2 (Fig. 3G) at cellular front were also dependent on clathrin, Hrs and AP-2, but not on AP-1, confirming that the recruitment of actin polymerizing proteins at the LE of migrating T cells depend on the presence of clathrin. Note that in Figure 3D–G only cells with ICAM-3 accumulation at the uropod, a hallmark of cell polarization responding to the chemokine were analyzed. The amount of cells with ICAM-3 recruited at the uropod was similar in control and silenced cells (Supporting Information Fig. 1).

Clathrin play a major role in T-cell polarization in response to SDF-1α

One major issue controlling ameboid migration is cellular polarization, which is driven at least partially, by actin

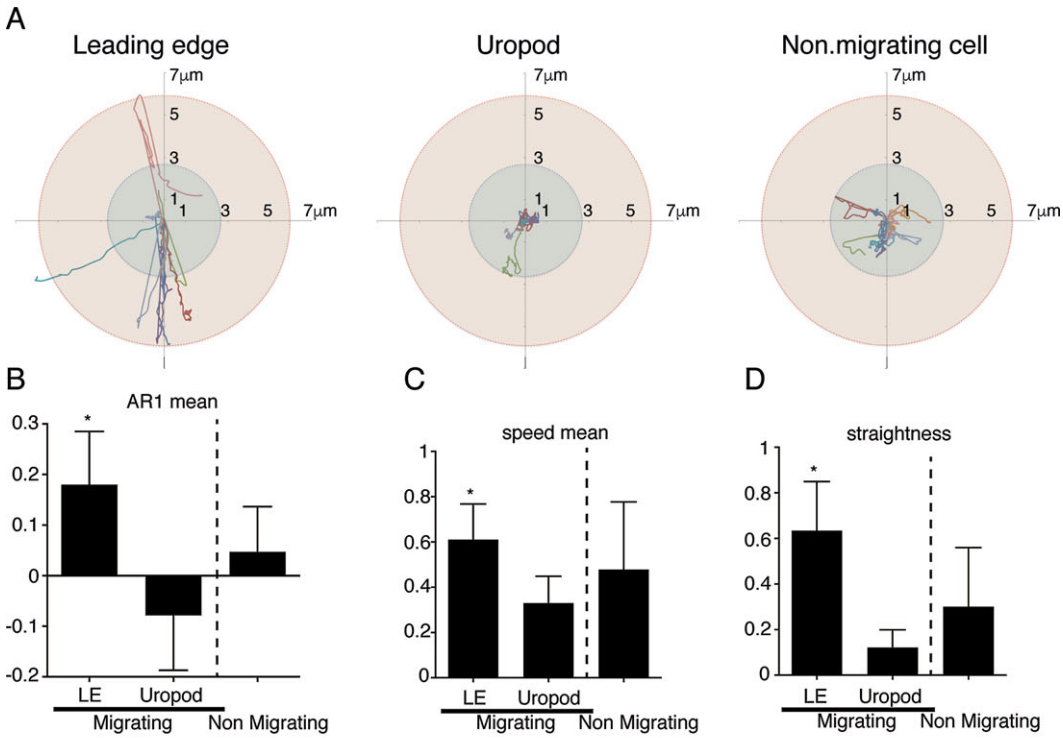

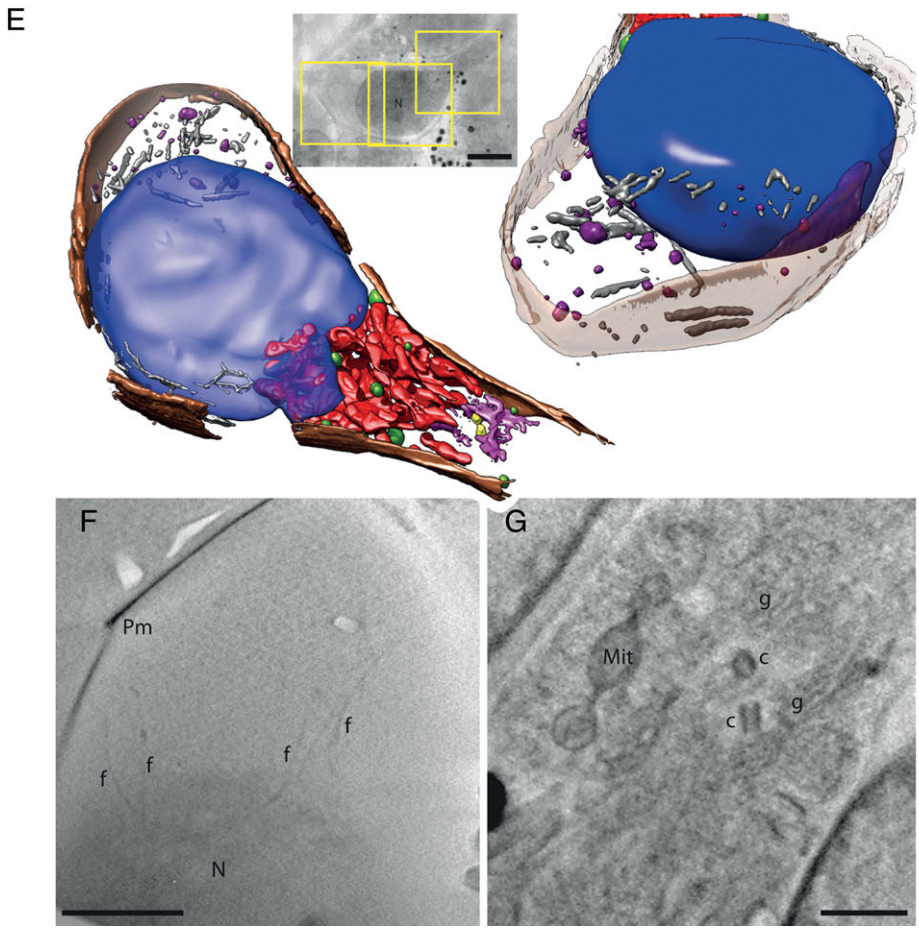

rearrangements [23]. In order to study whether clathrin, and clathrin associated to internal vesicles, plays a role in such polarization, we developed a novel image analysis software (FluoJ), also running in the ImageJ platform, that is able to automatically detect the individual cells and distinguishes their shape (Fig. 4A). This software is described in detail in the Methods section. From each individual cell, the software quantifies different predefined parameters such as the circularity, and therefore we are able to automatically analyze hundreds of individual cells, detecting polarized cells, avoiding human bias. Typical images of cell detection in control and clathrin (clathrin heavy chain [CHC]) silenced cells are shown (Fig. 4A, right panels). The frequency distribution observed between control and clathrin-silenced cells resulted different with almost 50% of control cells polarized after SDF-1α addition, in comparison with 25% of clathrin-silenced cells (Fig. 4B). The differences resulted more drastic in the hyperpolarized population; 6% of control cells and 1% in clathrin-silenced ones (Fig. 4B). Similar results were observed in Hrs-silenced cells (Fig. 4C), which showed a reduction in the population of polarized cells compared with control cells. These data confirm the role of clathrin and more specifically of clathrin associated to MVBs in actin-dependent T-cell polarization during migration.

Clathrin play a major role in chemotaxis-induced T-cell migration

In order to test whether clathrin silencing (which resulted in reduction of actin polymerization at the LE and cellular polarization) affects the migratory capacity of T cells, we performed classical lymphocyte trans-well chemotaxis assays. Briefly, T cells were plated over the top chamber of a trans-well plate, separated by a polycarbonate-coated membrane, allowing the passage of migrating T cells, from the lower chamber filled with medium containing SDF-1α. T cells were allowed to migrate toward the lower chamber and counted. When clathrin was silenced, we recovered 50% less cells from the bottom chamber (migrated cells) compared with control cells (Fig. 4D). Similar results were obtained when Hrs or AP-2 were silenced (Fig. 4D). On the contrary, nonsignificant results were obtained comparing control and AP-1 silenced cells. The effect of clathrin and Hrs in T-cell migration was also tested using the Jurkat cell line with similar results (Fig. 4E). In addition, we also tested whether clathrin could drive cellular migration in a 3D matrix. For that, cells were embedded in a collagen matrix and exposed to SDF-1α gradient. 3D migration was highly compromised in clathrin-silenced cells compared with control ones (Fig. 4F). Similarly, Hrs reduction also affects cellular migration in 3D collagen matrix (Fig. 4F). Note that no toxic effects were detected comparing control and silenced cells.

Primary T-cell migration is also dependent on clathrin

To ascertain whether clathrin play a major role in T-cell migration in a more physiological setting, we used peripheral blood lymphocytes (PBLs) isolated from human blood. PBLs resulted more polarized in presence of SDF-1α, and we observed more migrating cells compared to what observed using CEM cell line (data not shown).

We next tested whether silencing of clathrin or clathrin adaptors (Supporting Information Fig. 2A) impeded plasma membrane endocytosis needed for further vesicle trafficking toward the LE of migrating lymphocytes. With this purpose, the cell membranes of migrating PBLs were stained with a non permeable plasma membrane marker (CellMask Orange, Life Technologies), and after 20 min (the range of time for cell migration typically used in this study), the stain was washed away and the amount of fluorescence inside individual cells was quantified. Clathrin, or clathrin adaptors, silencing did not impede membrane uptake (Supporting Information Fig. 2B). As control, we used PBLs that were allowed to migrate longer times (1 h) after staining. They showed reduced membrane internalization when clathrin was silenced. However, Hrs silencing did not affect PBLs membrane internalization capacity (Supporting Information Fig. 2C).

The presence of endogenous clathrin, localized in both the uropod and the LE of migrating primary T cells, together with actin was assessed by fluorescence microscopy (Fig. 5A). Similar distribution pattern was also observed for Hrs and dynamin (Fig. 5B and C). Colocalization analysis shows that clathrin (Fig. 5D) and Hrs (Fig. 5E) from primary cells colocalized with actin at the LE but not in the uropod, confirming that clathrin (and clathrin associated to internal vesicles) interacts with actin at the front of migrating PBLs. Cellular migration was also impeded in clathrin- and Hrs-silenced cells (Fig. 5F), confirming again the role of clathrin in primary T-cell migration. In order to test whether the reduction in cellular migration resulted from a defect in actin accumulation, we analyzed actin accumulation at the LE by image analysis of fluorescent confocal images using the "FluorescenceRatio" software. As shown in Figure 5G, clathrin silencing reduces actin accumulation at the LE. Similarly, silencing of clathrin adaptors AP-1, AP-2,

Figure 2. Vesicle tracking in uropod and LE. (A) Human cell line CEM was transfected with td-Tomato-LCA in order to track clathrin-coated vesicles. Cell was seeded over human fibronectin-coated plates and stimulated or not with SDF-1α and imaged in a wide-field microscope. Vesicle tracking was analyzed in the LE and the uropod in migrating cells, or whole cells in nonmigrating ones. (B–D) Autoregressive mean of order 1 (B), speed mean (C), and straightness (D) are shown. (B–D) Data are shown as mean ± SD ($n = 30$) pooled from four independent experiments. (E) Cryo-soft X-ray tomography of a migrating T-cell. Top inset show the analyzed cell and the yellow squares represent the three adjacent tomograms acquired. Scale bar: 5 μm. On the left and right there are volumetric representations of the cell. Blue: nucleus; brown: plasma membrane; yellow: centriole; pink: Golgi apparatus; red: mitochondria; purple: vesicles; gray: filaments, N: nucleus. (F) Slide from a reconstructed tomogram from the LE showing filaments (f). Pm: plasma membrane. Scale bar: 2 μm. (G) Central plane of the uropod with the MTOC ("c" points to the centriole). Surrounding MTOC, "g" marks the position of the Golgi apparatus and Mit a mitochondria. Scale bar, 1 μm. Images are representative of three independent experiments.

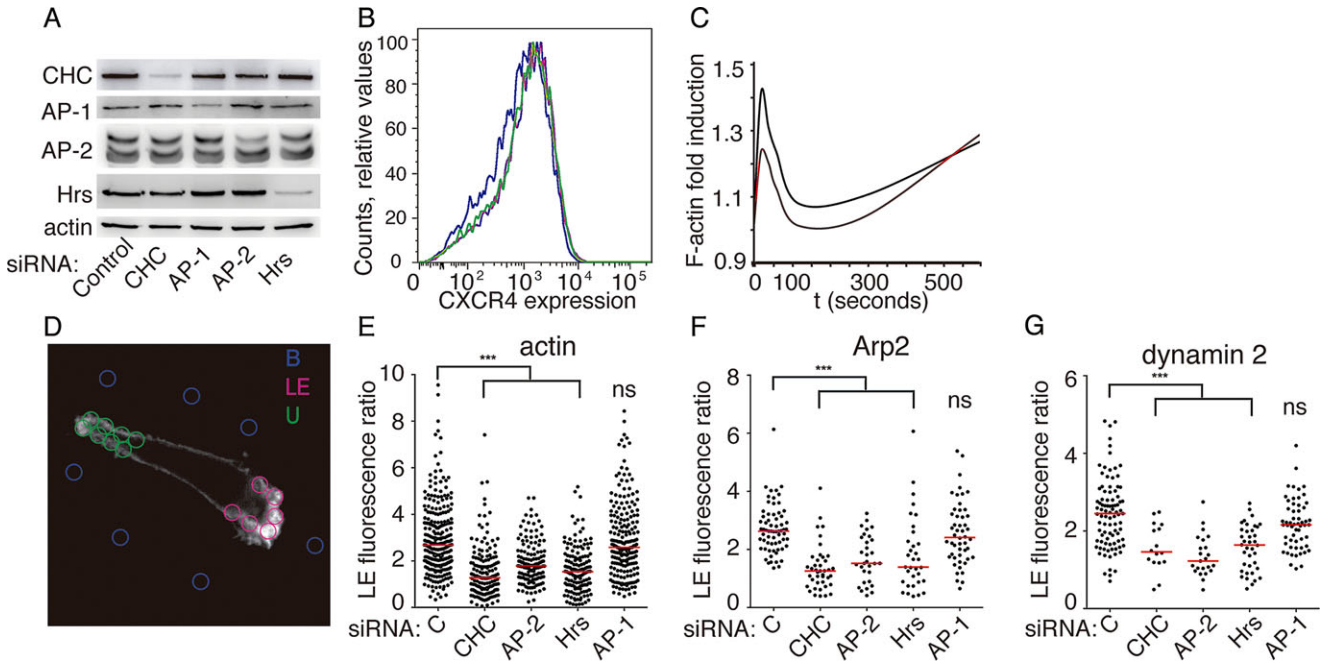

Figure 3. Clathrin and clathrin adaptor proteins are necessary for the recruitment of actin polymerizing machinery at the LE of migrating lymphocytes. (A) Protein (clathrin heavy chain and clathrin adaptors Hrs, AP-1 and AP-2) silencing by siRNA was analyzed in CEM cells by Western blotting. Blots are representative of 15 independent experiments. (B) CXCR4 (SDF-1α receptor) expression was tested by flow cytometry. CXCR4 expression in control cells (green line), Hrs (blue) and clathrin (magenta) silenced cells are shown. Data shown are representative of three independent experiments, with $n = 10^4$ events. (C) Actin polymerization dynamics in control or clathrin-silenced CEM T cells exposed to SDF-1α was tested by flow cytometry. F-actin content is expressed relative to time zero. One representative experiment of three is shown with control cells (black line) and clathrin heavy chain silenced cells in red. (D) To measure actin accumulation at the LE of migrating lymphocytes, we used ad hoc developed software "fluorescent ratio" comparing the fluorescence at the LE (circles in magenta) versus fluorescence in the uropod (circles in green). The fluorescence of the background was also taken into account (blue circles). (E–G) Actin (E), Arp2 (F), and dynamin 2 (G) accumulation at the LE was analyzed as shown in (D) in control cells as well as in cells silenced for the indicated proteins. Data are representative of at least three independent experiments (eight in the case of E). Significant differences ($p < 0.05$), analyzed by ANOVA followed by Dunn's multiple comparison test, are shown by *.

and Hrs also reduced the amount of clathrin accumulated at the LE. The accumulation of dynamin 2, and Arp2/3 complex was also compromised in clathrin and clathrin adaptors silenced PBLs (Fig. 5H and I).

Discussion

All these data show compelling evidence that clathrin, similarly to what is observed in T cells during the formation of the IS [10], plays a major role in actin accumulation at the LE of migrating lymphocytes. Clathrin silencing resulted in a reduction of arp2/3 and dynamin recruitment. Arp2/3 is the main actin nucleator and dynamin 2, can cross-link numerous protein adaptors than finally would activate Arp2/3 [24]. In addition, dynamin 2 is one the known proteins that links clathrin and actin polymerization (via cortactin) [16]. We, therefore, think that clathrin-coated membranes provide a support for the recruitment of the molecular platform that initiates actin polymerization at the LE of migrating lymphocytes. By regulating actin rearrangements, clathrin also controls lymphocyte polarization and migration. Note that the first steps of polarization are not impeded in situations of clathrin reduction, that is, ICAM-3 still polarized to the uropod, which indicates that the signal-inducing polarization, including the membrane receptors triggering this signaling, are not affected. Clathrin (or clathrin adaptors) silencing, however, dramatically reduces the hyperpolarized population, corresponding to the migratory cells.

Reducing the levels of clathrin and clathrin adaptors would indirectly affect migration by inhibiting the endocytic traffic and therefore membrane accumulation at the LE. However, the global membrane uptake at different time points was not disturbed in clathrin or in clathrin adaptors silenced cells (Supporting Information Fig. 2B). Therefore, these data obtained with the amoeboid migration of lymphocytes model confirm the intense relation of clathrin and clathrin-related proteins with the molecular machinery controlling actin rearrangements. Actin plays a major role in lymphocyte migration (and polarization) by controlling the dynamics of the cell shape during migration [25, 26]. Here, we show a model that integrate the motility signals triggered by the chemokines into coordinated actin rearrangements, being clathrin a key protein in this process that recruits the molecular machinery able to promote actin polymerization, similarly to what was observed in other biological processes [6, 10, 27].

We used different lines of human T cells as well as primary PBLs (T, B, and NK cells), indicating that this is a general mechanism

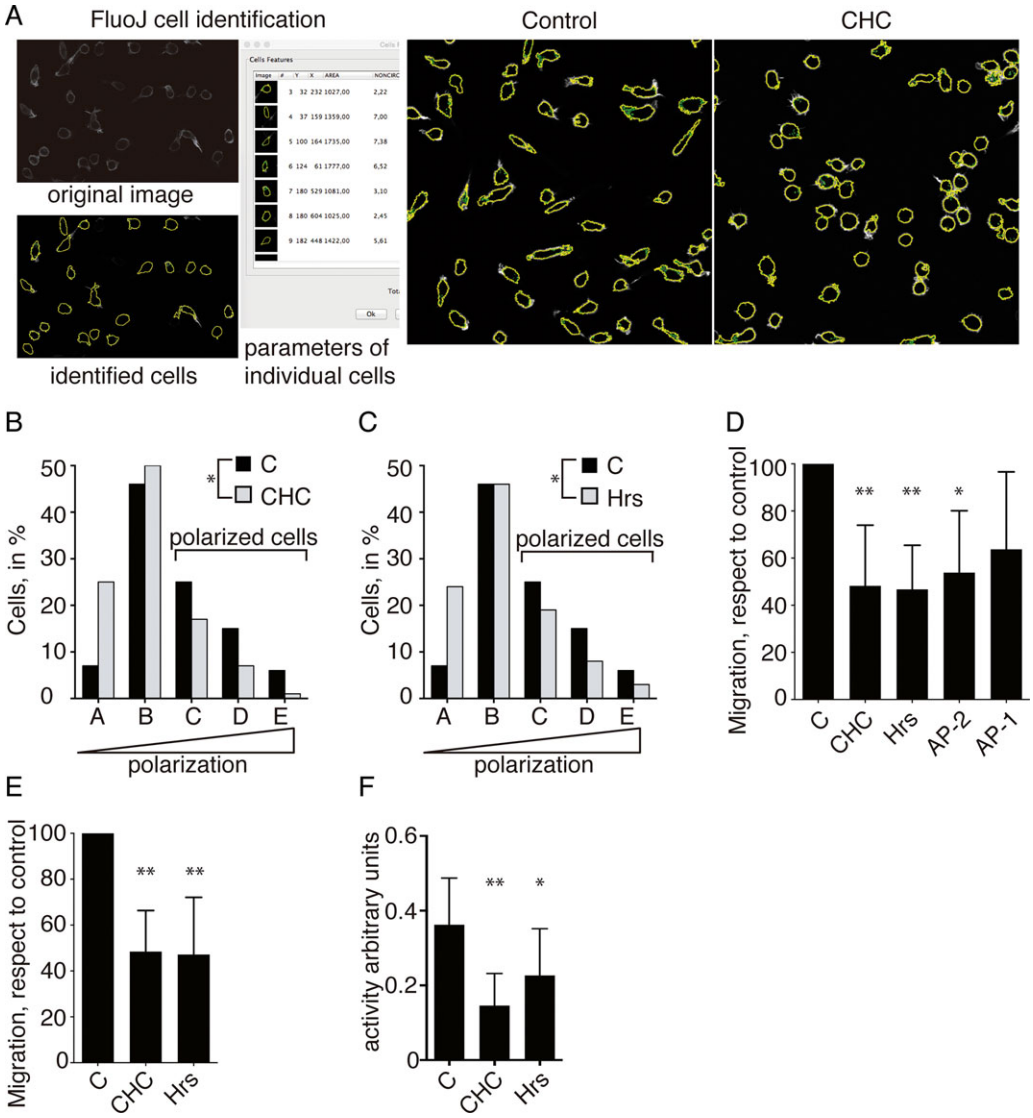

Figure 4. Clathrin deficiency affects cellular polarization and migration in 2D and 3D. (A) CEM cells were imaged by confocal microscopy and analyzed with FluoJ, a homemade software able to automatic cell identification. The software is able to identify and analyze different morphological parameters of each individual cell. An example of typical images of control and clathrin (CHC) silenced cells grown in the presence of SDF-1α is shown. Images are representative of eight independent experiments. (B–C) Histograms representing the cell polarization analysis of the whole population of CHC (B) or Hrs (C) silenced cells compared with control -C- cells. (D) Trans-well migration assays of control or silenced for the indicated proteins CEM cells. (E) As (D) by using J77 cells. (F) 3D migration assays of CEM cells (control, CHC- and Hrs-silenced) using μ-Slide Chemotaxis 3D chambers. (B and C) Data are pooled from eight independent experiments. (D–F) Data are shown as mean ± SD ($n = 10^4$) and are representative pooled from at least three independent experiments. Significant differences ($p < 0.05$), analyzed by ANOVA, followed by Dunn's multiple comparison test, are shown by *.

at least for cells of the lymphoid lineage. Whether this mechanism applies also to other amoeboid migrating cells, such as myeloid cells, deserve future research.

There are several differences regarding migration in primary cells compared to cell lines. Primary cells, which are more migratory, were more polarized and show a dependence on clathrin adaptor AP-1 that was not observed in cell lines. This can reflect the need for more clathrin-coated membranes, that independently of the population, that is, associated to the plasma membrane, MVB, or Golgi, can promote actin polymerization. In addition, this heterogeneity suggests that any membrane containing clathrin could be a support for actin polymerization during lymphocyte migration.

Materials and methods

Cells lines

The acute human leukemia Jurkat J77cl20 Vβ8 T and CEM cell lines were cultured in RPMI 1640 (Thermo Fisher, MA, USA)

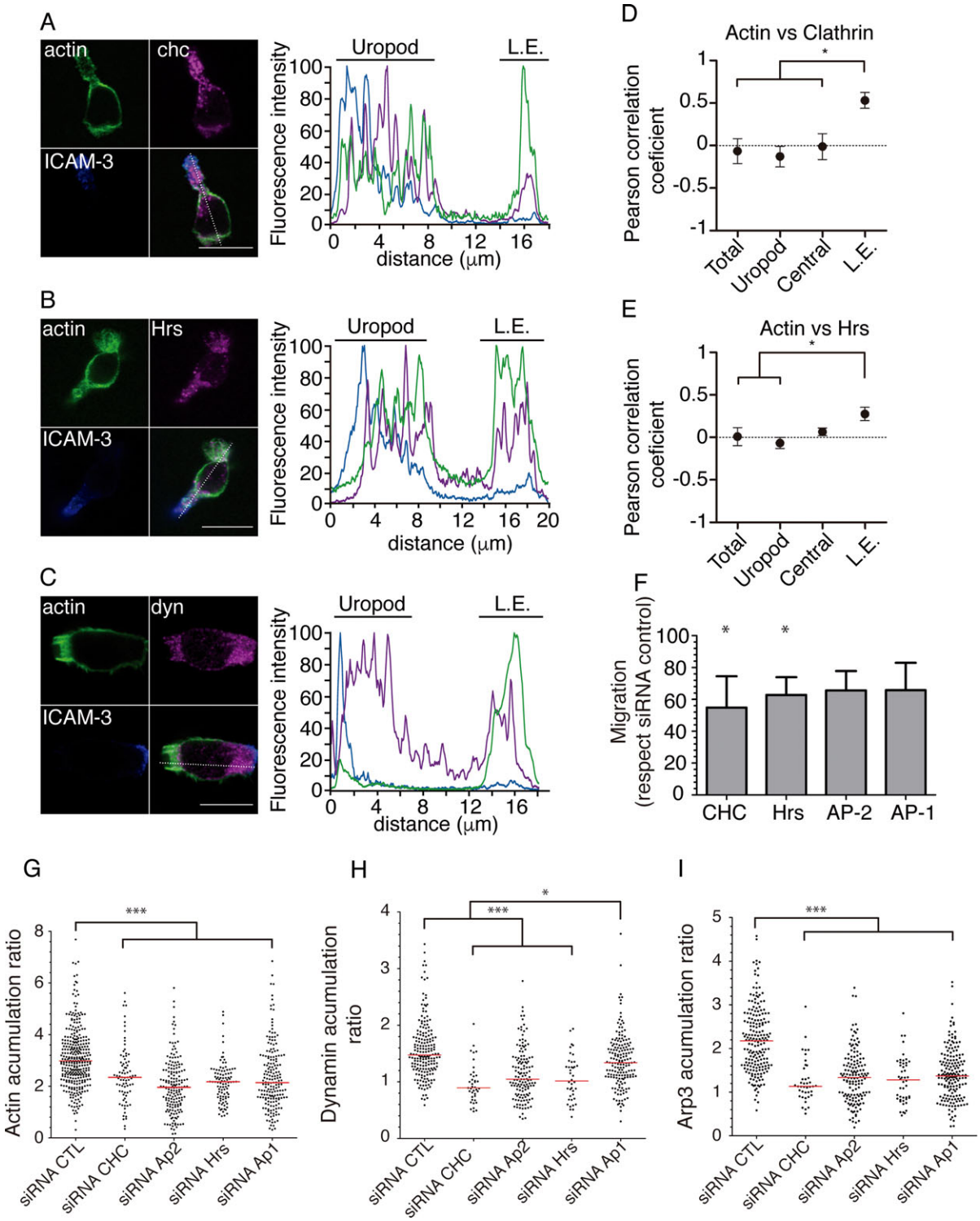

Figure 5. Clathrin localizes at the LE and drives actin accumulation in primary human lymphocytes. (A–C) Human PBLs were stained (uropod is marked with ICAM-3) for the indicated proteins and (left) imaged by confocal microscope (F-actin was detected using fluorescent phalloidin). (Right) Fluorescence intensity from uropod to LE was measured over the line represented at the merged images. Scale bar: 10 μm. Data are representative of four independent experiments. (D–E) High magnification confocal images were used for colocalization analysis of actin and clathrin (D) and actin and Hrs (E). (F) Trans-well migration assays of cells silenced for the indicated proteins. The results are represented with respect to migration in control cells (100%). Data are shown as mean ± SD A minimum of 10e5 cells were analysed, pooled from six independent experiments. Significant differences ($p < 0.05$), analyzed by ANOVA, followed by Dunn's multiple comparison test, are shown by *. (G–I) Actin (G), Arp2 (H), and dynamin 2 (I) accumulation at the LE was analyzed in control cells as well as in cells silenced for the indicated proteins. Data are pooled from five independent experiments. Significant differences ($p < 0.05$), analyzed by ANOVA, followed by Dunn's multiple comparison test, are shown by *.

supplemented with 10% fetal bovine serum (Thermo Fisher) and 100 U/mL penicillin (Thermo Fisher), 100 μg/mL streptomycin (Thermo Fisher).

Primary cells

Human peripheral blood mononuclear cells (PBMCs) were isolated from buffy coats (blood concentrates) obtained from healthy donors by separation on a Lymphoprep (Nycomed, Oslo, Norway) gradient according to standard procedures. Monocytes were purified from PBMC by a 30 min adherence step at 37°C in RPMI medium (HyClone, GE Healthcare Life Sciences, UK) supplemented with 10% fetal calf serum. Human T cells were purified from PBMCs, and were stimulated with 0.5 μg/mL phytohemaglutinin (Thermo Fisher, MA, USA) during 48 h followed by extensive washing. After this step, every 2–3 days 20 U/mL human recombinant IL-2 (R&D Systems, MN, USA) was added. Studies were performed according to the principles of the Declaration of Helsinki and were approved by the local Ethics Committee for Basic Research; informed consent was obtained from all human volunteers.

siRNA electroporation

Clathrin expression was reduced by transfection of Jurkat, CEM, or PBLs cells with either a dsRNA directed against clathrin heavy chain (sense [s] 5′-GGC CCA GGU GGU AAU CAU Utt-3′; antisense [as] 5′-AAU GAU UAC CAC CUG GGC Ctg-3′; IDT, Coralville, IA, USA) or with an On-Target SMART pool against clathrin heavy chain (GE Dharmacon). AP-1 was knocked down with a single dsRNA sequence (s 5′-GUU AAG CGG UCC AAC AUU Utt-3′, as 5′-AAA UGU UGG ACC GCU UAA Ctt-3′). Two sequences were used to knock down AP-2 (s 5′-GUU AAG CGG UCC AAC AUU Utt-3′, as 5′-AAA UGU UGG ACC GCU UAA Ctt-3′ and s 5′-CGC AGA GGG UAU CAA GUA Utt-3′, as 5′-AUA CUU GAU ACC CUC UGC Gtt-3′). Hrs was knocked down either with a pair of RNA sequences (s 5′-CGA CAA GAA CCC ACA CGU Ctt-3′, as 5′-GAC GUG UGG GUU CUU GUC Gtt-3′ together with s 5′-AAG CGG AGG GAA AGG CCA CUUtt-3′, as 5′-AAG UGG CCU UUC CCU CCG CUUtt-3′), or with an On-Target SMART pool (HGS) from (Dharmacon). Control sequences were On-Target plus nontargeting siRNA 1 and 2 (Dharmacon) or the sequence s 5′-UUC UCC GAA CGU GUC ACG Utt-3′, as 5′- ACG UGA CAC GUU CGG AGA Att-3′. All dsRNAs were purchased from Ambion (Thermo Fisher, MA, USA), IDT, or Dharmacon. Typically 20×10^6 cells and 1 μM siRNA were mixed in 400 μL Optimem (HyClone, GE Healthcare Life Sciences, UK). Electroporation were performed using a Gene Pulser II electroporation system (Bio-Rad, Hercules, CA, USA) at time constant mode, 240 V, 32 ms, and cuvettes of 4 mm. Cells were electroporated twice with a delay of 24 h. Cells were used for experiments on day 5 and silencing was confirmed by Western blot analysis.

DNA electroporation

We used 20 μg of the corresponding(s) plasmids for each condition (20×10^6 cells), in 400 μL in cuvettes of 4 mm of Optimem. For electroporation (Gene Pulser II electroporation system [Bio-Rad]), we used the time constant mode, 240 V, 32 ms. Cells were analyzed 24 or 48 h after transfection (depending on the tagged protein expression). Twelve or 24 h after electroporation, living cells were isolated by using Biocoll Separating Solution (Biochrom) by standard procedures. Plasmids encoding for td-Tomato-LCa, GFP–actin, dynamin–GFP and LifeAct–GFP were described elsewhere [10, 28–31]. CD63–GFP (cloned in pEGFP C1) was a gift from Dr. María Yañez Mo.

Immunolabeling

Lymphocytes were plated on slides coated with poly-L-lysine or fibronectin (Sigma-Aldrich, MO, USA) for 20 min at 37°C, fixed in PBS containing 4% paraformaldehyde (Electron Microscopy Sciences, Hatfield, PA, USA) during 20 min, and permeabilized with 0.5% Triton X-100 (Acros Organics, Thermo Fisher) in PBS (5 min) and then incubated with the indicated antibodies and revealed with Alexa-Fluor conjugated fluorescent secondary (Invitrogen, Thermo Fisher). Actin was stained with an Alexa-Fluor-conjugated phalloidin (Thermo Fisher). All samples were mounted in Prolong (Invitrogen, Thermo Fisher).

Confocal microscopy

Confocal images were obtained with a Leica TCS-SP5 confocal scanning laser unit with an inverted microscope (DMI6000B) under the control of Leica LAS AF Software. For living cell imaging, cells were plated onto fibronectin-coated (Sigma-Aldrich) 35 mm dishes (MatTek, MA, USA) and maintained at 37°C, 5% CO_2 inside an acrylic box covering the microscope. Images were analyzed using ImageJ software (NIH; Bethesda, MD, USA).

Migration assay: Trans-well

We used chambers separated by 5 μm polycarbonate filters (transwell permeable supports, Costar, NW, USA), allowing the passage of the migrating cells from the top chambers toward the bottom ones. In total, 0.5×10^6 cells were seeded in RPMI medium containing 10% FBS in the top chamber. The bottom chambers were filled with the same medium (RPMI/FBS) supplemented with 40 ng/mL SDF-1α. After 1 h at 37°C and in an atmosphere containing 5% CO_2, the top chambers were discarded and cells at the bottom medium were counted.

3D migrating assay

3D cell migration was performed using μ-Slide Chemotaxis 3D (IBIDI, Munich, Germany) following the instructions of the

manufacturer. These slides consist of two chambers (one of them filled with the chemo attractant; SDF-1α at 40 ng/mL) connected with another chamber containing the cells, which were embedded in Matrigel (BD Biosciences, CA, USA), forming a 3D matrix. Cells recognizing the chemo attractant move toward the chamber that contains SDF-1α. This slide was mounted in an inverted microscope (Leica TCS-SP5 confocal microscope) and images were acquired every 5 min. Images were analyzed using ImageJ (manual tracking and chemotaxis tool plugins).

Vesicle tracking

CEM cell line was transfected with td-Tomato-LCA. After 24 h transfection, cells were seeded over human fibronectin coated cover slides for 30 min. Cover slides were washed with PBS and imaged with a Leica Workstation AF 6000 LX equipped with an incubator box coupled to a CO_2 and calefactory unit (Pecon), Hamamatsu-1394ORCA-ERA-322079 camera, HCX PL APO 100× oil NA 1.4 objective and Leica filter N2.1. Data were processed with Imaris 6.0 software (Oxford Instruments, Oxford, UK).

Fluorescence ratio

To measure the ratio between the fluorescence of two different conditions, we follow an approach similar to the one described in [10]. We distinguish between three different regions: background alone (region A), condition 1 + background (region B), and condition 1 + condition 2 + background (region C). Let us refer to the fluorescence in each one of these regions as μ_0 (background), μ_1 (condition 1), and μ_2 (condition 2). The mean fluorescence observed in each region can be calculated as:

$$\begin{pmatrix} \mu_A \\ \mu_B \\ \mu_C \end{pmatrix} = \begin{pmatrix} 1 & 0 & 0 \\ 1 & 1 & 1 \\ 1 & 0 & 1 \end{pmatrix} \begin{pmatrix} \mu_0 \\ \mu_1 \\ \mu_2 \end{pmatrix}$$

from which we can easily solve for the fluorescence of each condition

$$\begin{pmatrix} \mu_0 \\ \mu_1 \\ \mu_2 \end{pmatrix} = \begin{pmatrix} 1 & 0 & 0 \\ 1 & 1 & -1 \\ -1 & 0 & 1 \end{pmatrix} \begin{pmatrix} \mu_A \\ \mu_B \\ \mu_C \end{pmatrix}.$$

The background-corrected fluorescence ratio between regions B and C is calculated as:

$$r = \frac{\mu_1 + \mu_2}{\mu_2}.$$

FluoJ

FluoJ is a computer workbench to partially automate fluorescence image processing workflows and facilitate the analysis and quantification of a large number of cells. We used it to process our sample with the goal of differentiating, polarized lymphocytes versus nonpolarized ones. The software has been developed in Java as an ImageJ plugin (TJ, 2007), software tool developed by the NIH and widely adopted by the scientific community. Installation (free) guide and information about the project can be found at http://biocomp.cnb.csic.es/twiki/bin/view/FluoJ.

In order to use FluoJ, the user goes through the following different stages: sample configuration, training (optional), and automatic image processing. We explain these stages in detail below.

1. Sample configuration. During this step, we define how to process images and register cell types. It starts with image preprocessing. This step allows us to define ImageJ commands to treat sample images before segmentation. In our case, 8-bit macro is used (to work on gray-level images this macro is always applied). Segmentation allows us to separate cells from background as well as regions of interest (ROIs) inside area for further processing. This process is illustrated in Supporting Information Figure 3A. It starts applying threshold macro, followed by Fill Holes (Supporting Information Fig. 3Ac–d). To separate superposed cells, Bright Margins is used; to detect ROIs, threshold is specified for ROIs (Supporting Information Fig. 5Ak). After segmentation, cells are registered with its corresponding points and ROIs. An example of image processing resulting from these configurations is displayed in Figure 4A.
2. Training. After sample configuration, the user can either train the classifier or directly enter into the automatic processing mode. During training, each cell is classified and stored in the database, together with its feature values (Fig. 4A and Supporting Information Fig. 3B). When several images have been processed and there are enough cells from each class, the classifier can be actually built. The classifier is a multiple-class naive Bayesian one, based on histograms of class descriptors obtained from the training data. Particle classification is performed by calculating the probability of observing the features actually measured for each possible particle type. The class maximizing the posterior probability is the one assigned to the particle. To evaluate results after training, manually classified particles are automatically classified. The confusion matrix (a matrix where each column represents the instances in a predicted class, while each row represents the instances in the actual class) and feature distributions for each class are displayed. Good features for classification must have dissimilar distributions for the different classes. The user can decide whether to keep on training or move forward to the automatic image processing step based on the results of this matrix. In our samples, we trained software until we reached 90% of accuracy (error below 10%).
3. Automatic image processing. During automatic image processing, data are registered and provided to the user (Fig. 4A) and can also be exported to plain text files. Additionally, a classification summary, with the number of particles detected for each class, and graphics with the particle features distribution are provided. We were able to process different sets of images and estimate polarization from classifier output. FluoJ provided an

easy-to-use framework to design and implement sample image processing workflow, minimizing human intervention. We were able to compare experimental and control data results, to measure features, to export data for further analysis with other software tools, etc.

F-actin determination

Levels of polymerized actin were measured as described [13]. Briefly, cells (1×10^5 per well of a 96-well plate) were incubated with 40 ng/mL SDF-1α at 37°C for the indicated times. Cells were then fixed, permeabilized, and stained with Phalloidin-Alexa 647 (Invitrogen). Fluorescence intensity was determined in a FACSCanto flow cytometer (BD Biosciences) and analyzed with Flow-Jo Software Ashland (OR, USA). Results are expressed as the fold increase in mean fluorescence intensity relative to the cells not exposed to SDF-1α.

Western blot

Western blot was performed using standard procedures. Primary antibodies used were the following: mouse monoclonal anti-CHC (abcam; Cambridge, MA, USA), rabbit polyclonal anti-CHC (abcam), rabbit polyclonal anti-Hrs (abcam), mouse monoclonal anti Ap1 (Sigma), mouse monoclonal anti-Ap2 (AP50, BD Biosciences Pharmigen), and mouse monoclonal anti-β-Actin (Sigma). Peroxidase-conjugated goat anti-mouse IgG and goat anti-rabbit were from Thermo Scientific.

Statistical analysis

Statistical analysis and comparisons were made with Graphad Prism (Graph Pad software, La Jolla, CA, USA). Differences between means were tested by Student's *t*-test for normal data. When analyzing more than two groups, we used one-way analysis of variance (ANOVA), and multiple mean comparisons were corrected with Bonferroni posttest. Differences were considered significant at $p \leq 0.05$. Data are shown in column bars representing the mean ± SD of at least three independent experiments unless otherwise indicated.

Soft-X-ray tomography

CEM cells were seeded on gold quantifoil R 2/2 holey film microscopy grids (Au-G200F1) coated with poly-L-lysine and allowed to migrate for 30 min in RPMI medium containing 40 ng/mL SDF-1α. Samples were vitrified by plunge freezing in a Leica EM CPC. Vitrified grids were transferred to Mistral (ALBA light source) [32, 33] beamline in ALBA synchrotron. For image acquisition, we used X rays with 520 eV photon energy, and X-ray projections taken at liquid nitrogen temperature with 1° tilt steps. The zone plate objective has an outermost zone width of 40 nm; tilt series alignment reconstruction and segmentation were performed as described in [34]. We used USFC Chimera software to join the three tomograms (Supporting Information Fig. 2) reconstruction generating a whole cell final tomogram.

Membrane cell staining

PBLs cultured in RPMI + 10% FBS and antibiotics (E/P) were seeded over polylysine-covered cover slides. Cells were maintained at 37°C and 5% CO_2 over 20 min. After 20 min every glass is washed twice with PBS, and then PBS + cell mask (1:1000 diluted) is added in order to stain the membranes over 15 min (at 37°C + 5% CO_2). Then, glasses are washed with RPMI + FBS and antibiotics twice. After the last wash, we add RPMI + FBS + antibiotics and SDF-1α to every glass. After the addition of the SDF-1α medium, we fix the cells at different times with PFA at 4%. Fluorescence emission was measured by confocal microscopy. The fluorescence inside individual cells was quantified from their central focal plane. At least 80 cells per condition were analyzed in three independent experiments.

Acknowledgments: This work was supported by the grants from the Spanish Ministry of Science and Technology (MICINN; BFU2011-29450 to E.V.) and Ministry of Economy and Competitiveness (MINECO; SAF2014-56716-REDT and BFU2014-59585-R to E.V., SAF2011-25834 to F.S.M., SAF2014-58895-JIN to A.C.A and BFU2014-54181-P to J.L.C.), the Madrid regional government (INDISNET-S2011/BMD-2332 to F.S.M.) and the European Research Council (ERC-2011-AdG 294340-GENTRIS to F.S.M.). We are grateful to the "Centro de Transfusión" of the "Comunidad Autónoma de Madrid" for providing the Buffy Coats.

Conflict of interest: The authors declare no commercial or financial conflict of interest.

References

1 **Ley, K., Laudanna, C., Cybulsky, M. I. and Nourshargh, S.**, Getting to the site of inflammation: the leukocyte adhesion cascade updated. *Nat. Rev. Immunol.* 2007. **7**: 678–689.

2 **de Bruyn, P. P. H.**, The amoeboid movement of the mammalian leukocyte in tissue culture. *Anat. Rec.* 1946. **95**: 177–191.

3 **Lämmermann, T., Bader, B. L., Monkley, S. J., Worbs, T., Wedlich-Söldner, R., Hirsch, K., Keller, M. et al.**, Rapid leukocyte migration by integrin-independent flowing and squeezing. *Nature* 2008. **453**: 51–55.

4 **Vicente-Manzanares, M. and Sánchez-Madrid, F.**, Role of the cytoskeleton during leukocyte responses. *Nat. Rev. Immunol.* 2004. **4**: 110–122.

5 **Merrifield, C. J. and Kaksonen, M.**, Endocytic accessory factors and regulation of clathrin-mediated endocytosis. *Cold Spring Harb. Perspect. Biol.* 2014. **6**. DOI: 10.1101/cshperspect.a016733.

6 **Veiga, E. and Cossart, P.**, Listeria hijacks the clathrin-dependent endocytic machinery to invade mammalian cells. *Nat. Cell Biol.* 2005. **7**: 894–900.

7 **Veiga, E., Guttman, J. A., Bonazzi, M., Boucrot, E., Toledo-Arana, A., Lin, A. E., Enninga, J. et al.,** Invasive and adherent bacterial pathogens co-opt host clathrin for infection. *Cell Host Microbe* 2007. **2**: 340–351.

8 **Saffarian, S., Cocucci, E. and Kirchhausen, T.**, Distinct Dynamics of endocytic clathrin-coated pits and coated plaques. In Hughson, F. (Ed.), *Plos Biol.* 2009. **7**: e1000191. DOI: 10.1371/journal.pbio.1000191.g009.

9 **Gautier, J. J., Lomakina, M. E., Bouslama-Oueghlani, L., Derivery, E., Beilinson, H., Faigle, W., Loew, D. et al.**, Clathrin is required for scar/wave-mediated lamellipodium formation. *J. Cell Sci.* 2011. **124**: 3414–3427.

10 **Calabia-Linares, C., Robles-Valero, J., la Fuente de, H., Perez-Martinez, M., Martin-Cofreces, N., Alfonso-Perez, M., Gutierrez-Vazquez, C. et al.**, Endosomal clathrin drives actin accumulation at the immunological synapse. *J. Cell Sci.* 2011. **124**: 820–830.

11 **Paczkowski, J. E., Richardson, B. C. and Fromme, J. C.**, Cargo adaptors: structures illuminate mechanisms regulating vesicle biogenesis. *Trends Cell Biol.* 2015. **25**: 408–416.

12 **Owen, D. J.**, Linking endocytic cargo to clathrin: structural and functional insights into coated vesicle formation. *Biochem. Soc. Trans.* 2004. **32**: 1–14.

13 **Morlino, G., Barreiro, O., Baixauli, F., Robles-Valero, J., González-Granado, J. M., Villa-Bellosta, R., Cuenca, J. et al.**, Miro-1 links mitochondria and microtubule Dynein motors to control lymphocyte migration and polarity. *Mol. Cell. Biol.* 2014. **34**: 1412–1426.

14 **Wojcechowskyj, J. A., Lee, J. Y., Seeholzer, S. H. and Doms, R. W.**, Quantitative phosphoproteomics of CXCL12 (SDF-1) signaling. In Kashanchi, F. (Ed.), *PLoS ONE* 2011. **6**: e24918. DOI: 10.1371/journal.pone.0024918.s002.

15 **Samaniego, R., Sanchez-Martin, L., Estecha, A. and Sanchez-Mateos, P.**, Rho/ROCK and myosin II control the polarized distribution of endocytic clathrin structures at the uropod of moving T lymphocytes. *J. Cell Sci.* 2007. **120**: 3534–3543.

16 **McNiven, M. A., Kim, L., Krueger, E. W., Orth, J. D., Cao, H. and Wong, T. W.**, Regulated interactions between dynamin and the actin-binding protein cortactin modulate cell shape. *J. Cell Biol.* 2000. **151**: 187–198.

17 **Gomez, T. S., Hamann, M. J., McCarney, S., Savoy, D. N., Lubking, C. M., Heldebrant, M. P., Labno, C. M. et al.,** Dynamin 2 regulates T cell activation by controlling actin polymerization at the immunological synapse. *Nat. Immunol.* 2005. **6**: 261–270.

18 **Schuh, M.**, An actin-dependent mechanism for long-range vesicle transport. *Nat. Cell Biol.* 2011. **13**: 1431–1436.

19 **Schneider, G., Guttmann, P., Heim, S., Rehbein, S., Mueller, F., Nagashima, K., Heymann, J. B. et al.,** Three-dimensional cellular ultrastructure resolved by X-ray microscopy. *Nat. Methods.* 2010. **7**: 985–987.

20 **Nagasawa, T.**, CXCL12/SDF-1 and CXCR4. *Front. Immunol.* 2015. **6**: 1–3.

21 **Krause, M. and Gautreau, A.**, Steering cell migration: lamellipodium dynamics and the regulation of directional persistence. *Nat. Rev. Mol. Cell. Biol.* 2014. **15**: 577–590.

22 **Rougerie, P., Miskolci, V. and Cox, D.**, Generation of membrane structures during phagocytosis and chemotaxis of macrophages: role and regulation of the actin cytoskeleton. *Immunol. Rev.* 2013. **256**: 222–239.

23 **Niggli, V.**, Insights into the Mechanism for dictating polarity in migrating T-cells. *Int. Rev. Cell Mol. Biol.* 2014: **312**: 201–270.

24 **Gordon-Alonso, M. and Veiga, E.**, Actin dynamics at the immunological synapse. *Cell Health Cytoskelet.* 2010. **2**: 33–47.

25 **Parameswaran, N. and Gupta, N.**, Re-defining ERM function in lymphocyte activation and migration. *Immunol. Rev.* 2013. **256**: 63–79.

26 **Dupré, L., Houmadi, R., Tang, C. and Rey-Barroso, J.**, T lymphocyte migration: an action movie starring the actin and associated actors. *Front. Immunol.* 2015. **6**: 1704–1718.

27 **Humphries, A. C., Dodding, M. P., Barry, D. J., Collinson, L. M., Durkin, C. H. and Way, M.**, Clathrin potentiates vaccinia-induced actin polymerization to facilitate viral spread. *Cell Host Microbe* 2012. **12**: 346–359.

28 **Massol, R. H., Boll, W., Griffin, A. M. and Kirchhausen, T.**, A burst of auxilin recruitment determines the onset of clathrin-coated vesicle uncoating. *Proc. Natl. Acad. Sci. USA* 2006. **103**: 10265–10270.

29 **Boyer, L., Turchi, L., Desnues, B., Doye, A., Ponzio, G., Mege, J.-L. and Yamashita, M. et al.,** CNF1-induced ubiquitylation and proteasome destruction of activated RhoA is impaired in Smurf1-/- cells. *Mol. Biol. Cell.* 2006. **17**: 2489–2497.

30 **Cao, H., Garcia, F. and McNiven, M. A.**, Differential distribution of dynamin isoforms in mammalian cells. *Mol. Biol. Cell* 1998. **9**: 2595–2609.

31 **Riedl, J., Crevenna, A. H., Kessenbrock, K., Yu, J. H., Neukirchen, D., Bista, M., Bradke, F. et al.**, Lifeact: a versatile marker to visualize F-actin. *Nat. Methods* 2008. **5**: 605–607.

32 **Pereiro, E., Nicolás, J., Ferrer, S. and Howells, M. R.**, A soft X-ray beamline for transmission X-ray microscopy at ALBA. *J. Synchrotron Radiat.* 2009. **16**: 505–512.

33 **Sorrentino, A., Nicolás, J., Valcárcel, R., Chichón, F. J., Rosanes, M., Avila, J., Tkachuk, A., Irwin, J., Ferrer, S., Pereiro, E.**, MISTRAL: a transmission soft X-ray microscopy beamline for cryo nano-tomography of biological samples and magnetic domains imaging, *J. Synchrotron Radiat.* 2015. **22**: 1112–1117.

34 **Cruz-Adalia, A., Ramirez-Santiago, G., Calabia-Linares, C., Torres-Torresano, M., Feo, L., Galán-Díez, M., Fernández-Ruiz, E. et al.**, T cells kill bacteria captured by transinfection from dendritic cells and confer protection in mice. *Cell Host Microbe* 2014. **15**: 611–622. Available from http://linkinghub.elsevier.com/retrieve/pii/S1931312814001401.

Abbreviations: **IS**: immunological synapse · **LE**: leading edge · **MVB**: multivesicular body · **ROI**: region of interest · **SDF-1α**: stromal cell derived factor 1α

Full correspondence: Dr. Esteban Veiga, Centro Nacional de Biotecnología (CSIC), Instituto de Investigación, Sanitaria Hospital de la Princesa, Hospital de Santa Cristina, Darwin 3, E-28049 Madrid, Spain
Fax: +34 915202374
e-mail: eveiga@cnb.csic.es

Received: 7/1/2016
Revised: 7/6/2016
Accepted: 6/7/2016
Accepted article online: 13/7/2016

